16 June 1995

ELSEVIER

Chemical Physics Letters 239 (1995) 230–236

CHEMICAL PHYSICS LETTERS

A new method for numerical flux calculations in quantum molecular dynamics

Gil Katz [a,b], Roi Baer [a,b], Ronnie Kosloff [a,b]

[a] *Department of Physical Chemistry, the Hebrew University, Jerusalem 91904, Israel*
[b] *The Fritz Haber Research Center, the Hebrew University, Jerusalem 91904, Israel*

Received 24 January 1995

Abstract

The flux of an evolving wavepacket is the definite time integral of its probability current density. A new method for calculating the flux, based on a Chebychev polynomial expansion of the quantum evolution operator is presented. The central point of the development is that the time integration of the current density is performed analytically, resulting in a scheme which eliminates additional numerical errors. Using this method, one benefits from both the time-dependent and time-independent frameworks of the dynamics. Furthermore, the method requires only a small modification to the existing Chebychev polynomial evolution code. Examples of performance and accuracy and an application to the calculation of recombinative desorption probabilities of N_2 on Re are shown and discussed.

1. Introduction

The entire physical and chemical information concerning a molecular system is contained in the wavefunction. When a molecular system is in a non-stationary state it evolves in time, and a corresponding evolution of the wavepacket will take place. Mathematically, the wavepacket evolves according to the Schrödinger equation,

$$i\hbar \frac{d\Psi}{dt} = \hat{H}\Psi(t), \tag{1}$$

where the nuclear Hamiltonian is the sum of kinetic and potential energies given by

$$\hat{H} = \sum_m \frac{\hat{P}_m^2}{2M_m} + \hat{V}. \tag{2}$$

The performance of a quantitative analysis of the dynamical evolution and properties requires a three-stage process. First, the wavepacket and the operators are represented in a form accessible to computers. Next, the wavepacket evolution is simulated numerically. The last stage, which is actually the goal of the calculation, is to analyze the wavepacket evolution in terms of measurable quantities.

A comprehensive integration of these three stages in a single strategy is crucial for efficient, accurate and coherent analysis. Therefore, a representation which is suitable for all three stages is to be developed. It must represent the wavepacket accurately enough to reflect all the relevant information content, and it should yield itself easily to the application of the Hamiltonian operator. Finally it must enable an easy extraction of the dynamical particulars which are of interest.

In many applications, representing the wavepackets on a sufficiently dense spatial grid has the benefit of meeting all the above demands. It is well known

0009-2614/95/$09.50
SSDI 0009-2614(95)00499-8

that the wavepacket information can be accurately represented on such a grid and that fast and accurate application of both the potential and the kinetic energy operators are in hand – the first is diagonal on a spatial grid and the second can be achieved using fast Fourier transform (FFT) algorithms [1]. For a diverse variety of problems grid methods can be easily applied in order to extract dynamical, physical and chemical information from the wavepacket grid representation [2,3].

The fast application of the Hamiltonian operator to a wavepacket represented on a grid enables the use of uniform polynomial approximations to functions of the Hamiltonian, most notably the evolution and Green function operators [4,5]. Thus, time evolution can be achieved on a grid. Since the Hamiltonian is a Hermitian operator, polynomial approximations can be used which have uniform convergence properties on a closed interval of the real line. One such approximation is the Chebychev polynomial expansion, which is by now widely used in many applications of molecular dynamics [6]. It has the benefits of accuracy, stability and simplicity.

Once on the move, the wavepacket's course is followed through the dynamical process, and its structure is analyzed in order to obtain quantitative information. This can be done by a variety of methods, most involve the application of projection operators. In many applications, however, a simple use of projection operators is not possible due to practical computational problems. A typical example appears in reactive scattering problems, where one is interested in the net wavepacket amplitude left in a certain region of the nuclear-configuration space after the reaction has ended. For instance, in a collision of the wavepacket with a potential barrier, the probability for reaction is obtained by determining the amplitude of the wavefunction in the asymptotic region beyond the barrier after the collision has ended.

This final wavepacket is usually widely spread since its amplitude is scattered in the various asymptotic reactive channels. Such a spread poses a practical problem – the need for a large grid extending vastly into the asymptotic regions of most reactive channels. Practically, however, there is no real need to spread a grid deep into the asymptotic regions, since these regions have no effects on the reaction mechanism. Thus the grid can terminate at the asymptotic region. In order to avoid boundary effects of this abrupt grid termination, the use of a negative imaginary potential (NIP) is usually recommended [7]. A properly constructed NIP has the capability of absorbing wavepacket amplitudes which reach the grid boundaries with almost no reflection or transmission [7–12]. The amount of final wavepacket amplitude in the various asymptotic channels cannot be determined by projection operator methods, since by the time the collision has ended, this amplitude, together with others, has been absorbed by the NIPs. Thus what is needed is a dynamical counter which integrates the amplitude flowing into the asymptotic region, before it is absorbed by the NIPS. This is accomplished by using the integral of the flux, that is, the current density is integrated over the entire reaction time and then spatially over a surface perpendicular to the reaction coordinate in an asymptotic channel to yield the total probability of reaction via that channel.

While the spatial integration is easily and accurately performed on the grid points – by a simple summation – the time integration can present problems. One way is to perform the time evolution in short time steps and to simply sum the flux over time. This method has the drawback of poor accuracy and requires short time steps. Since the Chebychev scheme is especially efficient for long time steps, this method is usually inappropriate.

In this Letter, a proper method to integrate the flux over time is presented, a method in the spirit of the Chebychev propagation scheme. It is based on the fact that the Chebychev series separates time from space. The time variable appears in well-known analytical functions, such as Bessel functions and exponentials, and therefore time-only manipulations can be done without any reference to the evaluation of the temporary wavepacket: they should be done before the application to wavepackets, and if possible, analytically. This approach to the Chebychev expansion can be utilized in other applications, and can yield convenient expansions for various operators. This idea is not new. Kosloff [2] showed that the time integral needed for the calculation of molecular absorption spectra can be worked out analytically – yielding a new Chebychev polynomial whose coefficients are themselves Chebychev polynomials.

Recently Kouri and co-workers [5] used this same series to expand the Green function of the Hamiltonian, thus obtaining 'time-independent' wavepackets.

The integration method presented in this Letter was discovered [13] while developing a numerical algorithm for calculating the sensitivity functions of observables to the underlying potential energy surface. The time-dependent equation for sensitivity functions developed by Baer and Kosloff [13,14] involved the evaluation of the time integral of the product of two evolving wavepackets, and a scheme closely analogous to the one presented here was then used. In this Letter the method is described in detail and its characteristics and performance are tested. The organization of the Letter is as follows. The current density integration scheme is presented in Section 2. Some of the tests performed are shown in Section 3. An application of the scheme for the calculation of recombinative desorption probabilities is presented in Section 4.

2. The current density time-integration scheme

For completeness the essentials of the Chebychev expansion of the evolution operator are outlined, which can be written as the following series [3,9]:

$$\Psi(\tau, R) = \mathrm{e}^{-\mathrm{i}\hat{\omega}\tau} \sum_{n=0}^{N} a_n(\nu\tau)\phi_n(R). \tag{3}$$

The coefficients of the expansion, $a_n(\nu\tau)$ are proportional to the nth Bessel functions $J_n(x)$, more specifically $a_n(x) = (2 - \delta_{n0})J_n(x)$. The symbols $\phi_n(R)$ denote the functions obtained by operating with $T_n(\hat{H}_N)$ on the initial state $\Psi(0)$, where $T_n(x)$ are the Chebychev polynomials. This operation can be carried out recursively using the well-known recurrence relation of the Chebychev polynomials,

$$\phi_{n+1} = -2\mathrm{i}\hat{H}_N\phi_n + \phi_{n-1}. \tag{4}$$

The recurrence is initiated by setting $\phi_0 = \Psi(0)$ and

$$\phi_1 = -\mathrm{i}\hat{H}_N\phi_0. \tag{5}$$

The normalized Hamiltonian $\hat{H}_N$ is a shift-and-scaled version of the original Hamiltonian operator, enforcing the Hamiltonian eigenvalues into the $[-1, 1]$ domain. The original Hamiltonian eigenvalue limits can be easily evaluated since the effect of the grid is to restrict the highest value of the momentum to the highest representable frequency – $P_i^{\max} = \pi/\Delta x_i$. Thus the eigenvalues of the original Hamiltonian reside in the interval $[E_{\min}, E_{\max}]$, where $E_{\min}$ is the minimum value of the potential energy on the grid $V_{\min}$, and $E_{\max} = \Sigma_n (P_n^{\max})^2/2M_n + V_{\max}$. The shift-and-scaled Hamiltonian is then given by

$$\hat{H}_N = (\hat{H} - \hat{\omega})/\nu, \tag{6}$$

where $\hat{\omega} = \frac{1}{2}(E_{\max} - E_{\min})$ and $\nu = \frac{1}{2}(E_{\max} + E_{\min})$.

The current density of a wavepacket Ψ at a certain nuclear configuration $\boldsymbol{R}$ is the expectation value of the operator $\hat{\boldsymbol{J}}(\boldsymbol{R}) = \frac{1}{2}\Sigma_m M_m^{-1}[\hat{\boldsymbol{P}}_m\delta(\hat{\boldsymbol{R}} - \boldsymbol{R}) + \delta(\hat{\boldsymbol{R}} - \boldsymbol{R})\hat{\boldsymbol{P}}_m]$ given by the well-known expression

$$\boldsymbol{J}(t) = \frac{1}{\hbar M}\mathrm{Im}[\Psi^*(t)\nabla\Psi(t)], \tag{7}$$

where, for simplicity of notation, the explicit reference to $\boldsymbol{R}$ and the summation over the different nuclei of the molecule (the summation over m) are omitted. The integrated flux $\boldsymbol{F}(\boldsymbol{R}, t)$ is obtained by integrating $\boldsymbol{J}$ over time: $\boldsymbol{F}(t) = (\hbar M)^{-1}\ \mathrm{Im}[\boldsymbol{I}(t)]$, where

$$\boldsymbol{I}(t) = \int_0^t \Psi^*(\tau)\nabla\Psi(\tau)\ \mathrm{d}\tau. \tag{8}$$

The proposed method exploits the fact that the Chebychev polynomial expansion of the evolution operator (Eq. (3)) is actually a series which separates the time variable from the spatial variables. The time variables in this series appear in well-known analytical forms, such as Bessel functions and exponentials, so that the time integration can be made analytically. Unfortunately, in our case using this idea in a straightforward way, that is plugging Eq. (3) twice into Eq. (8) yields a time integral of two Bessel functions for which we could find no convenient analytical expansion. We did notice, however, that if we think of one of the $\Psi(\tau)$ in Eq. (8) as a backward evolution of $\Psi(t)$ rather than a forward evolution of $\Psi(0)$, we can make use of the following analytical property of Bessel functions [15]:

$$\int_0^x J_n(x-y)J_m(y)\ \mathrm{d}y = 2\sum_{k=0}^{\infty}(-1)^k J_{n+m+2k+1}(x). \tag{9}$$

Representing $\Psi(\tau)$ as a backward evolution of $\Psi(t)$ means using the following expansion:

$$\Psi^*(\tau) = e^{i\hat{\omega}(\tau - t)} \sum_{n=0}^{N} a_n(\nu(\tau - t))\chi_n^*(R), \quad (10)$$

where $\chi_n(R)$ are given by the operation of the nth Chebychev polynomial T_n on $\Psi(t)$. Inserting the expansion of Eq. (3) to represent $\Psi(\tau)$ and the expansion of Eq. (10) to represent $\Psi^*(\tau)$ into Eq. (8) yields the following expression for $I(t)$:

$$I(t, R) = \frac{2}{\nu} e^{-i\hat{\omega}t} \sum_{n,m} (-1)^m (2 - \delta_{n0})(2 - \delta_{m0}) \times A_{m+n}(\nu t)\chi_m^*(R)\nabla\phi_n(R), \quad (11)$$

where the coefficients $A_{n+m}(x)$ are defined as

$$A_{m+n}(x) = \tfrac{1}{2}\int_0^x J_m(x - y)J_n(y)\,dy = \sum_{k=0}^{\infty} (-1)^k J_{n+m+2k+1}(x). \quad (12)$$

Since the number N of terms in the Chebychev polynomial expansion is chosen so that $J_n(\nu t)$ is negligible for all $n > N$, the 'infinite' summation in Eq. (12) can be truncated, once $2k$ reaches the value $N - (m + n + 1)$.

The numerical implementation of this algorithm is shown in Fig. 1. The first time step (A in the figure) establishes the wavefunction $\Psi(t)$. This wavefunction must now be propagated both forward in time – step B – and backwards (for calculation of $\chi_m^*(R)$ in Eq. (12)) – step B′. It should be noted that the same Chebychev functions $\phi_n(R) = T_n(H_N)\Psi(R, t)$ are needed for both these propagations, thus eliminating almost completely the additional computation effort. This algorithm computes the flux (in a given direction) in all points in space. If only the flux through a given surface is needed, storage can be saved and the flux can immediately be integrated on the desired surface, as it is formed. The procedure is then repeated to the next time step. Overall, the additional computational effort required for the calculation of flux (in a given direction) is that of a spatial directional derivative per Hamiltonian operation. The extra storage is not large since the flux is accumulated only on a dividing plane separating the interaction region and the products.

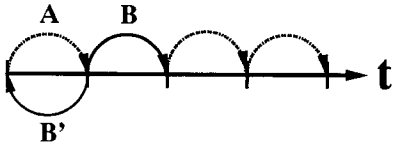

Fig. 1. A schematic view of the sequence of applying the flux integration in the Chebychev evolution procedure. The total time is divided into smaller segments. Step A is the initiation step. Step B and B′ are executed simultaneously, using the same Chebychev functions.

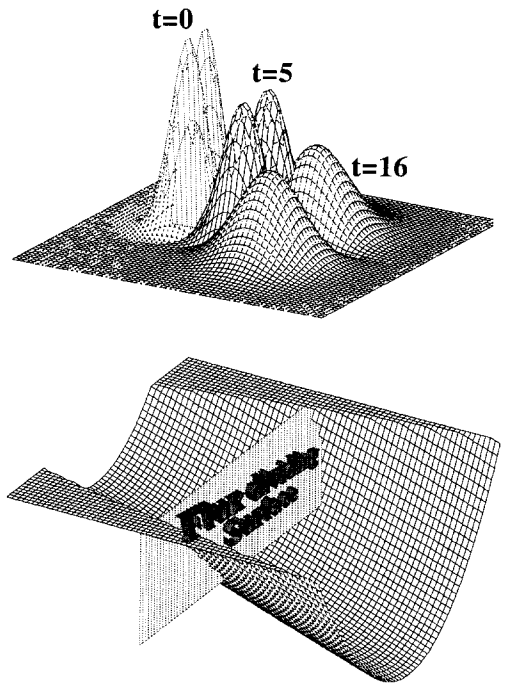

Fig. 2. Top: three snapshots of the wavepacket at $t = 0$, $t = 5$ and $t = 15$. Bottom: The trough shaped potential surface and the flux dividing surface (here, a plane). A grid of 64×64 points was used with $\Delta x = 0.313$ and $M = 1$.

3. Testing the algorithm

In order to test the algorithm, a wavepacket was propagated on a two-dimensional potential energy surface shaped as a trough with a tilting slope toward the right-hand side (see Fig. 2). This potential energy surface eventually forces an initial wavefunction to leave the grid. To eliminate artificial boundary effects, an appropriate NIP was placed on the right-

hand side of the grid. The initial wavepacket was chosen as a Gaussian in the translation coordinate and the $v = 1$ vibrational eigenvalue in the perpendicular coordinate. Fig. 2 shows the potential surface used and three snapshots of the propagating wavepacket.

The flux was calculated at two different dividing planes on the grid, the first is shown superimposed on the potential surface in Fig. 2. Due to the structure of the potential a wavepacket positioned to the left of the flux planes will eventually cross them both at different times. Since all the wavepacket amplitude eventually leaves the grid passing through the dividing planes, the flux in this calculation should accumulate to one. This is shown in Fig. 3.

The dominant source of computational error is the representation of momentum on the spatial grid. Once the grid spacing is chosen correctly, however, the results converge to computer accuracy. The time integration introduces practically no additional computational errors. This is shown in Table 1 where the asymptotic value of the accumulated flux is shown for different time steps and Chebychev series lengths. In principle, one could use even larger time steps (we obtained converged results up to $\Delta t = 0.6$ and $n = 128$), but this is limited in this case because of the presence of a non-Hermitian NIP term in the Hamiltonian, which causes the Chebychev expansion to become unstable for larger time steps [16].

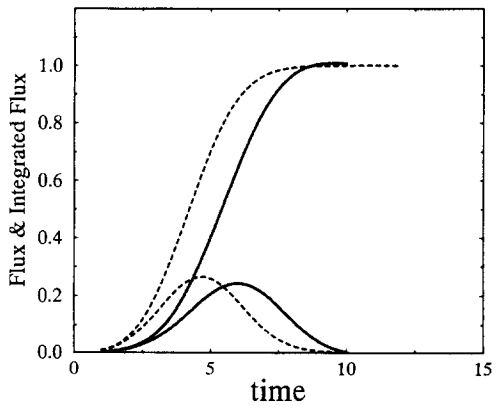

Fig. 3. The crossing rate and accumulated probability of crossing two dividing planes located at $x = 8.76$ (dashed) and $x = 9.696$ (solid). Starting on the left at $t = 0$, the wavepacket crosses first the left plane and then the right. At $t = 16$, practically all amplitude has crossed both surfaces and the accumulated crossing probabilities reaches its asymptotic limit of 1.

Table 1
The integrated flux obtained versus the time step Δt and the number of expansion coefficients N in Eq. (3)

N	Δt	Integrated flux
4	0.1	0.7863304969002306
8	0.2	0.9996801964320893
16	0.2	0.9999735160206360
32	0.2	0.9999999999996339

4. Application to recombinative desorption

Recombinative desorption is a process taking place on a crystal surface where dissociated adsorbed atoms assemble to create a molecule which then leaves the surface. The process can be modeled as taking place on two potential surfaces, an inner potential describing the adsorbed atoms and a physisorption potential describing the molecular physisorption well which leads to the dissociated species. The two potentials are coupled by a nonadiabatic coupling potential V_{12}. The potential is a modification of the potential used in Ref. [17] which amounts to closing the dissociation channel and is shown in Fig. 4 (see Table 2).

To model the process, a wavefunction is positioned on the inner potential. As time passes part of the wavefunction will cross into the outer potential which leads to desorption. Fig. 4 shows a model potential describing the recombinative desorption of N_2 on a Re surface. Superimposed on the potential is the evolving wavepacket. The initial wavepacket is vibrationally hot in the mode perpendicular to the surface.

Fig. 4 shows the evolution of the wavepacket where only a small portion is able to escape. The mean energy of the wavefunction is 2 kJ/mol below the barrier crossing point, therefore the process proceeds by tunneling. From an experimental point of view the internal energy distribution of the desorbing molecule is of interest. To obtain this information, the flux into the asymptotic internal eigenstates is calculated. This is done by first projecting the wavefunction on the flux dividing plane (which is perpendicular to the translational coordinate Z) on an

asymptotic eigenfunction and then integrating the flux by the procedure described above.

Fig. 5 shows the flux into the individual vibrational levels of N_2, showing only a small amount of vibrational excitation. This finding is in accordance with the picture obtained from the reverse process of dissociative adsorption of N_2 on Re where both experiment and calculation show that vibrational energy is less effective than translation in promoting the dissociation [17].

Table 2
Parameters of propagation in au

grid	$\Delta z = 0.06$	$\Delta y = 0.06$ $z_0 = 1.2$ $y_0 = 0.9$
physisorption grid	$N_z = 64$	$N_y = 64$
inner grid	$N_z = 64$	$N_y = 64$
time propagation	$\Delta t = 0.2$ (au)	$N_{ch} = 16$

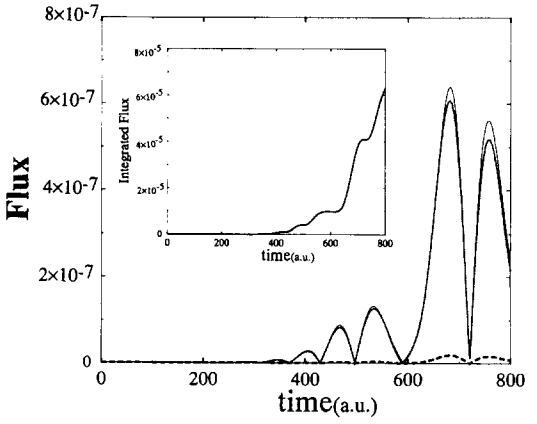

Fig. 5. The flux function as a function of time for the $v = 0$ (dashed) and $v = 1$ (bold dashed) asymptotic states. The total dissociative flux is shown as a solid line. The insert shows the integrated flux as a function of time. Notice that the flux arrives in waves.

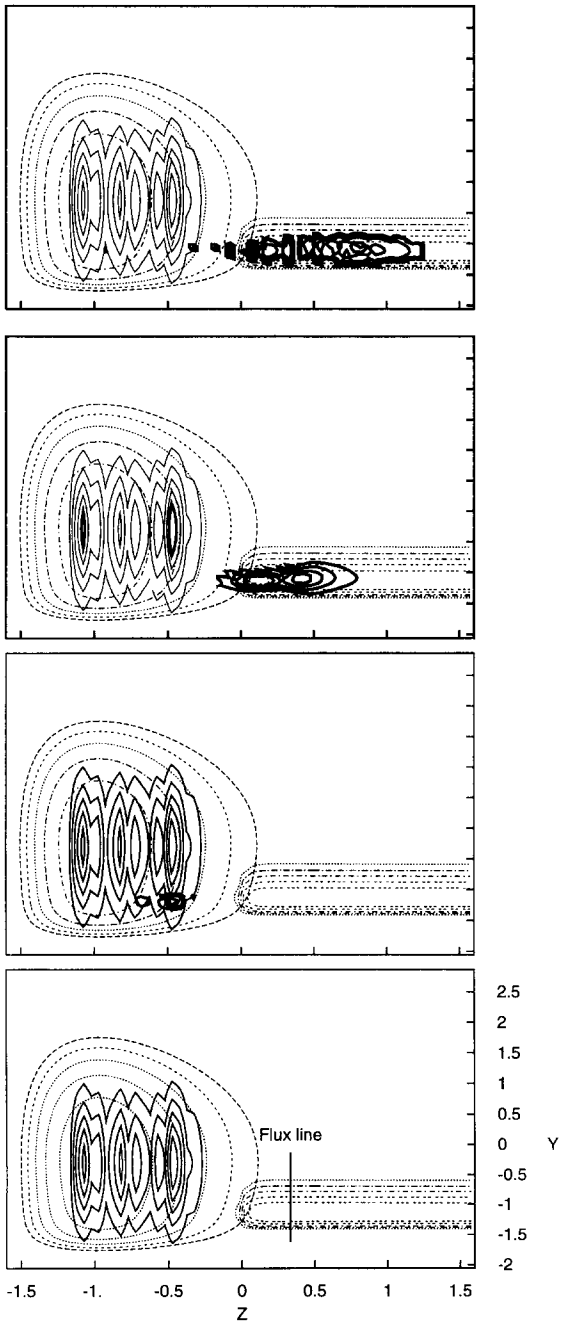

Fig. 4. Snapshots of a recombinative desorption event. The Z coordinate is perpendicular to the surface and the Y coordinate is the molecular N–N internuclear distance. The lower panel shows the wavefunction at $t = 0$ in the inner chemisorption potential. The flux dividing plane on which the flux is integrated to give the rate is displayed. The lower middle panel shows the wavefunction at time $t = 200$ au. Notice that a new wavefunction is born on the dissociative potential at the position of the outer turning point of the inner potential. The upper middle panel, $t = 400$ au, the dissociative wavepacket progresses down the exit channel. A more developed wavepacket is shown in the upper panel for $t = 1000$ au.

5. Conclusions

The increasing popularity of time-dependent quantum mechanical methods supplies the motivation to search for effective means to perform on-line analyses. In this work the integrated flux was studied as such an analysis tool. It was shown that the integrated flux to an individual asymptotic channel can be calculated with extremely high accuracy. Moreover, the flux analysis can supply causal information on the sequence of events that lead to a particular result.

From a qualitative viewpoint the flux vector is the closest analogue to the trajectory line in classical mechanics supplying the information on the direction of flow of a mechanical system. In this capacity it has been utilized as a qualitative tool from the early days of time-dependent grid methods [18–21]. The flux analysis is, therefore, a source of insight in the spirit of time-dependent quantum mechanical methods.

Acknowledgement

This research was supported by the German–Israel Foundation. The Fritz Haber Research Center is supported by the Minerva Gesellschaft für die Forschung, GmbH München, Germany.

References

[1] R. Kosloff, in: Numerical grid methods and their application to Schrödinger's equation, The Fourier method, ed. C. Cerjan, NATO ASI Ser. C 412 (Kluwer, Dordrecht, 1993).
[2] R. Kosloff, J. Phys. Chem. 92 (1988) 2087.
[3] R. Kosloff, Ann. Rev. Phys. Chem. 45 (1994) 145.
[4] R. Kosloff and H. Tal-Ezer, Chem. Phys. Letters 127 (1986) 223.
[5] Y. Huang, W. Zhu, D.J. Kouri and D.K. Hoffman, Chem. Phys. Letters 214 (1993) 451;
W. Zhu, Y. Huang, D.J. Kouri, C. Chandler and D.K. Hoffman, Chem. Phys. Letters 217 (1994) 73;
D.K. Hoffman, Y. Huang, W. Zhu and D.J. Kouri, J. Chem. Phys. 101 (1994) 1242.
[6] D. Neuhaser, M. Baer, R.S. Judson and D.J. Kouri, Comput. Phys. Commun. 63 (1991) 460;
D. Neuhauser, Chem. Phys. Letters 200 (1992) 173;
S.K. Gray, J. Chem. Phys. 96 (1992) 6543;
C. Iung, C. Leforestier and R.E. Wyatt, J. Chem. Phys. 98 (1993) 6722.
[7] G.G. Balint-Kurti and A. Vibok, in: Numerical grid methods and their application to Schrödinger's equation, Complex absorbing potentials in time dependent quantum dynamics, ed. C. Cerjan, NATO ASI Ser. C 412 (Kluwer, Dordrecht, 1993).
[8] C. Leforestier and R.E. Wyatt, J. Chem. Phys. 78 (1983) 2334.
[9] R. Kosloff and D. Kosloff, J. Comput. Phys. 63 (1986) 363.
[10] D. Neuhauser and M. Baer, J. Chem. Phys. 90 (1989) 4351.
[11] M.S. Child, Mol. Phys. 72 (1991) 89.
[12] A. Vibok and G.G. Balint-Kurti, J. Phys. Chem. 96 (1992) 7615.
[13] R. Baer and R. Kosloff, J. Phys. Chem. (1994), in press.
[14] R. Baer and R. Kosloff, Chem. Phys. Letters 200 (1992) 183.
[15] M. Abramowitz and I.A. Stegun, Handbook of mathematical functions (Dover, New York, 1972).
[16] Y. Huang, D.J. Kouri and D.K. Hoffman, J. Chem. Phys. 102 (1995), in press.
[17] E. Por, G. Haase, O. Citri, R. Kosloff and M. Asscher, Chem. Phys. Letters 188 (1991) 553.
[18] E.A. McCullough and R.E. Wyatt, J. Chem. Phys. 51 (1969) 1253; 54 (1971) 3578.
[19] R. Kosloff and Y. Zeiri, J. Chem. Phys. 97 (1992) 1719.
[20] D. Lemoine, J. Chem. Phys. 101 (1994) 4350.
[21] S.M. Miller and M.H. Alexander, J. Chem. Phys. 101 (1994) 8663.